Simple box model of nutrient fluxes in the Lower St. Lawrence Estuary

Mathilde Jutras[a,*], A Mucci[a], B Sundby[a], Y Gratton[b], S Katsev[c]

[a] *Earth and Planetary Sciences Department, McGill University, Montreal, QC, Canada*
[b] *Centre Eau Terre Environnement, Institut national de la recherche scientifique, Quebec, QC, Canada*
[c] *Large Lakes Observatory and Department of Physics, University of Minnesota Duluth, MN, USA*

1. Keywords

nutrient cycling; box model; St Lawrence; eutrophication; nutrients

2. Abstract

We present a simple linear three-box model of nutrient cycling in the Lower St. Lawrence Estuary (LSLE). A present-day nutrient budget is obtained for fixed-nitrogen, phosphorus, and silica, from which the model's parameters are derived. The model is used to (i) test the sensitivity of each layer's nutrient concentration to perturbations in nutrient and water volume inputs, (ii) obtain the response time of the system to a new steady state following a perturbation, and (iii) estimate bottom-water oxygen consumption. We find that most of the dissolved nutrients (70% of fixed-nitrogen, 90% of phosphorus) that reach the surface waters in the Lower Estuary originate from the deep waters, implying that the anthropogenic eutrophication potential of the St. Lawrence River is moderate. Our nutrient budget suggests that the Lower St. Lawrence Estuary acts as a nutrient pump for the Gulf of St. Lawrence. Nitrate appears as the limiting nutrient to surface productivity in the LSLE. This model can be used to test the impact of natural or anthropogenic perturbations on nutrient and oxygen concentrations in the LSLE.

3. Introduction

The Gulf of St. Lawrence and Estuary make up the largest estuarine system in the world (Fig. 1a). The St. Lawrence Estuary is supplied by freshwater flowing seaward from the Great Lakes and other tributaries, and by landward-flowing North Atlantic waters, entering the Gulf at depth through the Cabot and Belle Isle Straits. The estuary is therefore subject to both coastal and open ocean processes, and hosts a complex nutrient circulation.

Direct observations and proxy measurements have revealed that the dissolved oxygen concentrations in the bottom waters of the Gulf of St. Lawrence and Lower Estuary have decreased significantly over the past

*Corresponding author
Email address: mathilde.jutras@mail.mcgill.ca (S Katsev)

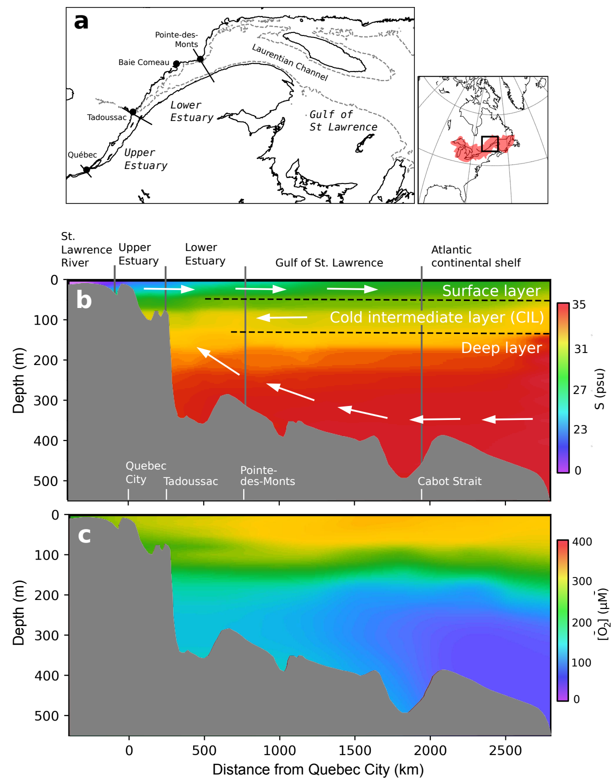

Figure 1: The St. Lawrence System. **a** Map of the St. Lawrence Estuary, showing the deep Laurentian Channel (LC). The dotted line shows the 150 m isobath. Red shows the extent of the drainage basin of the St. Lawrence System. **b** Schematic representation of the three layer stratification in the Lower St. Lawrence Estuary for a transect along the Laurentian Channel. Colors show practical salinity. Modified after Dickie and Trites (1983). **c** Transect of dissolved oxygen concentration along the Laurentian Channel. All data taken from the BioChem database.

80 to 100 years (Gilbert et al., 2005; Thibodeau et al., 2010). Minimum dissolved oxygen concentrations in the Lower St. Lawrence Estuary (LSLE) varied from ~ 150 μmol kg^{-1} in the 1930s to less than 60 μmol kg^{-1} since 1985 (Gilbert et al., 2005). About 2/3 of the oxygen depletion has been attributed to changes in the relative proportions of the two water masses that mix on the continental shelf and enter the Gulf through Cabot Strait: the cold, oxygen-rich Labrador Current waters and the warm, oxygen-poor North Atlantic Central waters (Gilbert et al., 2005). The remaining oxygen depletion is associated to local processes, such as an increase in microbial respiration promoted by increasing bottom-water temperatures (Genovesi et al., 2011) and eutrophication (Benoit et al., 2006; Thibodeau et al., 2006) - the bacterial oxygen consumption triggered by increased fluxes of organic matter to the deep waters following phytoplankton blooms promoted by anthropogenic nutrient and allochtonous organic matter exports. The St. Lawrence River drains highly populated areas - with associated discharge of waste waters to the river and its tributaries - and fertile lands that host intensive farming. These activities are the source of high nutrients and particulate organic matter (Hudon et al., 2017) whose export has increased substantially over the last decades (Clair et al., 2013; Marcogliese et al., 2015; Pocklington and Tan, 1987). A better understanding of the fate of these nutrients in the system is essential to assess the role of eutrophication on the observed bottom-water deoxygenation. In this paper, we present a simple box model to represent the flow of nutrients (N, P, Si) through the stratified LSLE, a model that informs us on how changes in the circulation and nutrient export affect the fate of nutrients and the oxygen demand in the Lower St. Lawrence Estuary.

Similar approaches have been used in the past, but over the whole St. Lawrence System (Savenkoff et al., 2001) and to look at bacteria (Painchaud et al., 1987). This model informs us on (i) the sensitivity of the system to perturbations, and (ii) the time required to reach a new steady-state following a perturbation. By solving the model for varying freshwater discharge and nutrient input concentrations, we calculate how nutrients redistribute in the water column. First, we describe the study area, the characteristics and boundary conditions of the model and how they were chosen, proceed to define the active processes, highlight the model parameters for which measurements exist, derive missing parameters, and finally describe how the model was solved, before presenting results of the current steady state and the Lower Estuary's response to a range of hypothetical scenarios.

3.1. Description of the system

The most prominent bathymetric feature in the Gulf of St. Lawrence and Lower Estuary is a deep ($>$ 250 m) U-shaped channel, the Laurentian Channel (LC), that stretches 1240 km from Tadoussac to the continental shelf break (Fig. 1). Tidal effects and seawater intrusions can be observed all the way to Quebec City, but the Lower St. Lawrence Estuary (LSLE) is defined as the section of the estuary that hosts this deep channel and extends from Pointe-des-Monts to Tadoussac.

The LSLE is strongly stratified and, throughout most of the year (ice-free season), is characterized by three distinct layers (see Fig. 1b and 9): (1) a 25-50 m deep, warm, low salinity, seaward flowing surface layer, a mixture of freshwater from various tributaries (mostly the St. Lawrence River) and seawater originating from the Gulf and Atlantic Ocean, (2) a cold, more saline intermediate layer, the Cold Intermediate Layer (CIL), found between 50 m and about 150 m depth, formed in the winter in the Gulf, and (3) a warmer, more saline deep layer, a mixture of North Atlantic and Labrador Sea waters that enters the Gulf through Cabot Strait after mixing on the shelf (Dickie and Trites, 1983; Galbraith, 2006; Savenkoff et al., 2001). At the head of the LSLE, near Tadoussac, the sill rises from 200 m to less than 100 m, leading to strong mixing, upwelling, and complex tidal currents (Gratton et al., 1988) that bring nutrient-rich deep waters to the surface. This region is characterized by high biological activity and sustains a large and diverse population of marine mammals.

4. Method

4.1. Model description

In this section, we will first describe the box model, and then the numerical analysis methodology. The chemical characteristics (e.g. nutrient concentrations) of the model are based on a large set of historical observations gathered over the last decade on the R/V Coriolis II and obtained through the BioChem database made available by the Department of Fisheries and Oceans Canada. The latter contains data from the Atlantic Zone Monitoring Program (AZMP) and from a number of other field samplings.

A box model typically requires that every box is well-mixed and uniform. As shown in Fig. 2, nutrient concentrations are relatively constant along isopycnals from Tadoussac to Pointe-des-Monts, and decrease seaward (especially at the surface). Below the surface layer, temperature is also relatively uniform along the LC. The bottom-water oxygen concentration decreases landward, but is relatively uniform from Baie-Comeau to Tadoussac. The relative uniformity of water properties (T, S) and nutrient concentrations along isopycnals in this 200-km section of the LC suggests that the LSLE section from Tadoussac to Baie-Comeau can realistically be represented by a box model provided that it is split vertically to reflect the physical (density) stratification.

Based on the common description of the LSLE and its physical stratification (Fig. 9abcd), three boxes would be needed to represent the system properly. Vertical nutrient profiles (Fig. 9efg) do not provide evidence for the presence of two distinct layers in the top 150 m of the LSLE, i.e. do not distinguish the surface from the CIL. Property-property diagrams (salinity against temperature and nutrient concentrations), for their part, show no distinction between the CIL and the deep layer (e.g. Fig. 10). Thus, taking into consideration the previous observations, we abide by the three-layer stratification and use 3 vertical boxes to represent the LSLE: a surface box with a depth of 50 m, an intermediate box with a depth of 100 m, and a deep box with a depth of 150 m (see Figure 3c).

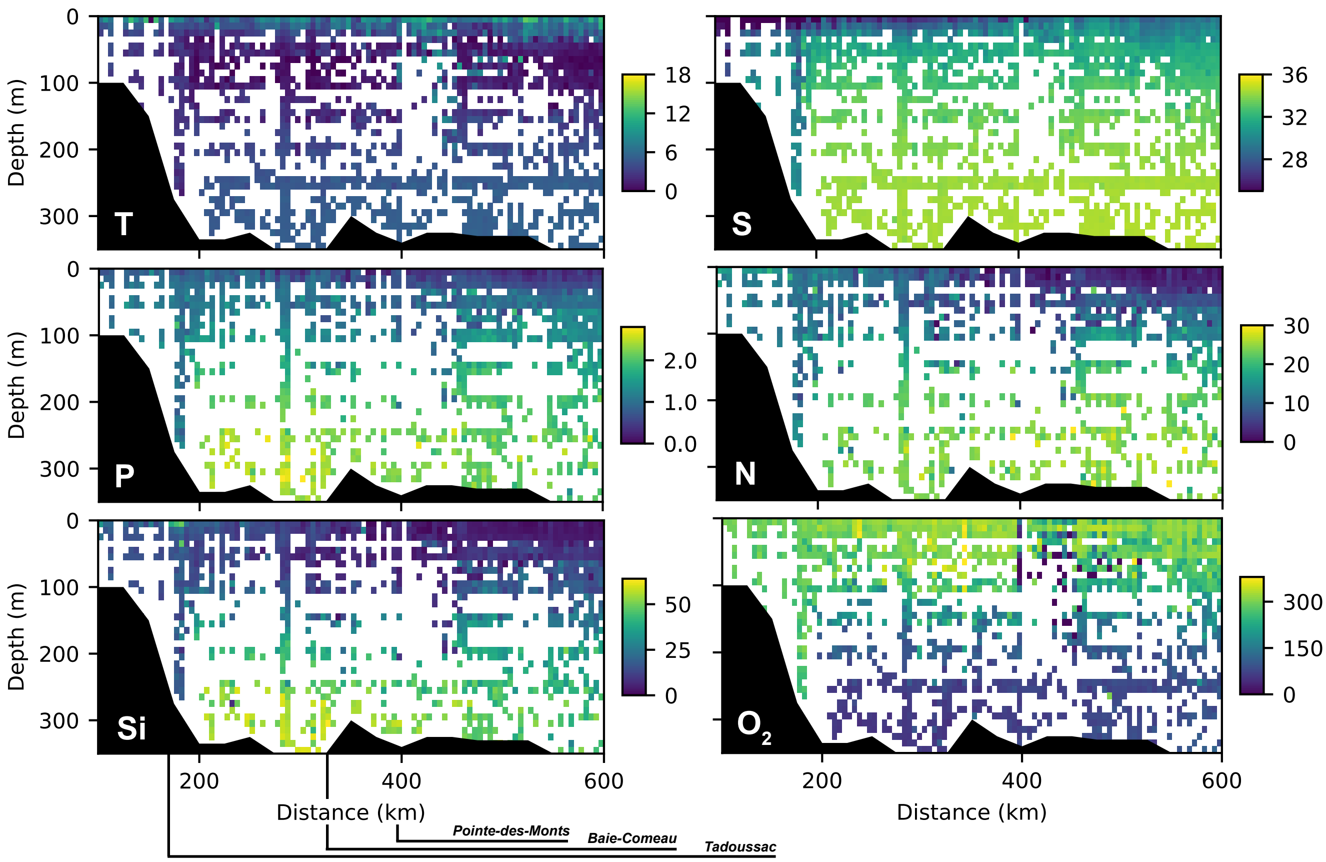

Figure 2: Transects of various physical and chemical properties along the LC (T = temperature, S_P = practical salinity, SRP = soluble reactive phosphate, dSi = dissolved silicate). The distance is in km from Quebec City. In every bin, the available data from 1990 to 2018 for the whole width of the estuary are averaged. Grey bins contain no data. Unless specified otherwise, all units are in μmol kg^{-1}. The inset shows the geographical location of available nitrate data from 1990 to 2018.

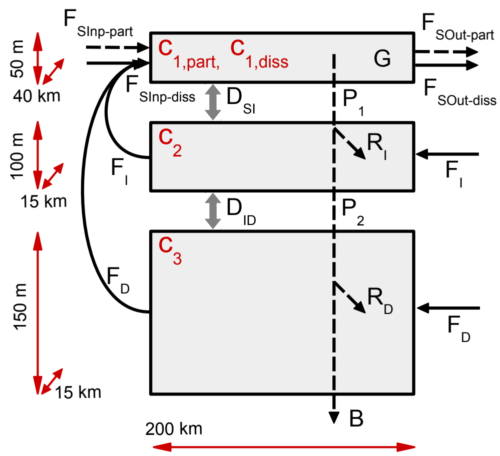

Figure 3: Box model. Each layer is characterized by a nutrient concentration c_i. The different flux terms are: S/S_i are the source/sink terms, in which solutes are transformed into particulate organic matter by photosynthesis and vice-versa (microbial particulate organic matter (POM) remineralization). F_i are the mass fluxes. D_{ij} are the turbulent diffusive terms. B is the burial rate to the sediments, and P_i are the POM gravitational settling rates. R_i are the remineralization rates, and G is the dissolved nutrient uptake rate (POM formation).

We consider that the volume of the boxes is fixed, meaning that the depth of the interfaces between the three boxes (or layers) does not vary with time. This model is therefore more representative of the summer conditions, since, in the winter, when the freshwater flow is minimal and heat is lost to the atmosphere, the surface layer deepens as it readily mixes with the CIL. Nevertheless, the mass balance stays the same throughout the year, and only the model's nutrient distribution is affected by seasonal changes.

The model is expressed in terms of fluxes and source/sink terms of nutrients in each box. Both the dissolved (available for biological uptake, Fig. 3a) and particulate (microbially metabolizable organic form, irrespective of their oxidation state, Fig. 3b) forms of nutrients are solved for. Transformation from one form to the other ensures total mass conservation.

The exchange mechanisms considered between the boxes are (i) lateral and vertical (upwelling) transport of dissolved and particulate nutrients (F_i terms on Fig. 3), (ii) particle settling (P_i), (iii) burial in the sediments (B), (iv) photosynthesis (or skeletogenesis) and microbial remineralization (or skeletal dissolution) in the water column (S/S_i,G,R_i), and (v) turbulent mixing (D_{ij}).

Assumptions and boundary conditions

Precipitation (rainfall) and evaporation, as well as inputs from rivers other than the St. Lawrence and Saguenay Rivers are neglected, as their contributions to the nutrient budget are relatively small. Nitrogen fluxes from the atmosphere and nitrogen fixation are also not considered, a reasonable since atmospheric deposition in the LSLE (3×10^8mol yr^{-1}, Prospero et al. (1996)) accounts for only 1.5% of the nitrogen input to the system (Hudon et al., 2017). Diffusion of nutrients out of the sediments is not explicitly resolved but is implicit to the model, since the only flux to sediments is *permanent* burial. We assume that only the dissolved forms of nutrients can be transported to overlying waters by upwelling and turbulent mixing, while the particulate forms are only subject to gravitational settling. Only the *net* flux associated with turbulence mixing (upwelling minus downwelling) is represented. Allochtonous particulate matter originates solely from the St. Lawrence and Saguenay Rivers. For our estimates of dissolved fixed-nitrogen, we neglect nitrite and ammonia, as their concentrations are, on average, 200 times lower than nitrate. The boundary conditions representing the circulation pattern mirror the overall flow, which is seaward at the surface and landward below. In reality, at the surface, a cyclonic gyre that sits east of Pointe-des-Monts takes water out of the Estuary along the South shore (Gaspé Current) and brings water in along the North shore. At the western boundary, upwelling brings water from the intermediate and deep layers to the surface.

In the Lower Estuary, upwelling and mixing rates are much higher near the western edge of the LC (i.e., head of the Laurentian Channel), because of the sudden shoaling of the seafloor landward of Tadoussac (from about 200 m to less than 100 m deep). Nevertheless, in each box, a single value for these parameters is used, as they represent the integrated averaged value over the box. Sediment trap estimates of biogenic particle settling rates show an increase landward along the Lower Estuary, as the contribution of terrigenous organic matter delivered by the St. Lawrence River increases (Benoit et al., 2006; Colombo et al., 1996). The particle flux used in the model is also an integrated average along the LSLE section of the LC.

Mathematical formulation

Readers who are not interested in the details of the model formulation can jump to section 5. The flux terms shown in Fig. 3 are defined in Table 1. Each process is defined as a linear function of nutrient concentrations, a reasonable assumption away from null and very high nutrient concentrations. More realistic functions may not be linear, in particular between the gravitational settling and POM concentration in the surface layer, or between POM formation and dissolved nutrient concentrations. Nevertheless, given the simplicity of our model and the lack of consensus about the formulation of such relations (Dunne et al., 2005; Kriest and Oschlies, 2008; Martin et al., 1987; Sarmiento and Gruber, 2006), linear relationships are applied.

The basic equations of this model are the sum of all fluxes in each layer. At steady state ($\frac{dc_i}{dt} = 0$), this leads to the following equations, where f_i represents volume fluxes, B permanent burial, E_i are the turbulent mixing coefficients, P_i are the particulate matter settling fluxes, and G is the transformation from the dissolved to particulate form (see Table 1). The subscripts *diss* and *part* refer to, respectively, the dissolved and particulate forms of nutrients, $SInp$ designates the surface input (from the upper estuary), $SOut$ is the surface output (i.e. into the Gulf), I is the intermediate layer input and D is the deep layer input. For concentrations c_i, the layers are identified from 1 (surface) to 3 (deep layer). From layer 1 to 3:

$$f_{SInp}c_{SInp,diss} - f_{SOut}c_{1,diss} + f_I c_2 + f_D c_3 + E_1\left(c_2 - c_{1,diss}\right) - G = 0 \quad (1)$$

Table 1: Flux terms of the box model and their mathematical formulations.

Term (mol s^{-1})	**Definition**	**Expression**
F_i	Water input/output	$F_i = f_i c_i$, where f_i is the water flux in $m^3 s^{-1}$ and c_i is the nutrient concentration of this water mass/layer.
D_{ij}	Mixing between layer i and j	$D_{ij} = E_{ij}\left(c_j - c_i\right)$, where E_{ij} is the turbulent mixing coefficient.
P_i	Particulate settling flux	$P_i = a_i c_{1,part}$, where $c_{1,part}$ is the particle concentration in the first layer and a_i is a flux coefficient with units m^3 s^{-1}, a fraction of the amount of particulate matter settling out of layer 1 reaching layer i.
B	Burial rate	The burial rate can be expressed as the fraction b of the biogenic particle flux exported from layer 1 that is permanently buried, or as $B = bc_{1,part}$ where b is a flux coefficient similar to a_i.
Other fluxes that can be calculated		
R_i	Remineralization	Amount of organic nutrient being remineralized (conversion from organic to inorganic form) and equal to $R_{i+1} = P_i - P_{i+1} = P_i - xP_i$ where x is the fraction of P_i remineralized in layer $i+1$.
G	Nutrient uptake	Amount of inorganic nutrient being transformed to its organic form by photosynthetic activity, equal to $G = f_{SInp}c_{SInp,part} - f_{SOut}c_{1,part} - P_1 = f_{SInp}c_{SInp,diss} - f_{SOut}c_{1,diss} + E_1(c_2 - c_1) + f_I c_2 + f_D c_3$. We consider a linear function between the uptake rate and the dissolved nutrient concentration, $G = \alpha c_{1,diss}$, where α is a coefficient of units ($m^3 s^{-1}$).

$$f_I c_I - f_I c_2 - E_1\left(c_2 - c_{1,diss}\right) + E_2\left(c_3 - c_2\right) + P_1 - P_2 = 0 \tag{2}$$

$$f_D c_D - f_D c_3 - E_2\left(c_3 - c_2\right) + P_2 - B = 0 \tag{3}$$

and for particulate material in the first layer:

$$f_{SInp}c_{SInp,part} - f_{SOut}c_{1,part} + G - P_1 = 0 \tag{4}$$

To ensure mass conservation, the particulate matter output flux is derived from the balance of all input fluxes which must be equal to zero, giving:

$$c_{1,part} = \frac{1}{f_{SOut}}\left[f_{Sinp}\left(c_{Sinp,diss} + c_{Sinp,part}\right) + f_I c_I + f_D c_D - f_{SOut}c_{1,diss} - B\right] \tag{5}$$

Again, to ensure mass conservation, we consider that all excess/lack of particulate/dissolved nutrient is due to a transformation from one form to the other.

Model formulation

The model is finally expressed with four equations to solve for the four nutrient concentrations ($c_{1,part}$, $c_{1,diss}$, c_2, c_3). All required parameters are presented in Tables A1 and 2. We use equations 1+4, 3, total mass conservation and the nutrient uptake relationships (Table 1).

$$\begin{aligned}
f_{SInp}(c_{SInp,part} + c_{SInp,diss}) - f_{SOut}(c_{1,part} + c_{1,diss}) + f_I c_2 + f_D c_3 + E_1(c_2 - c_{1,diss}) - a_1 c_{1,part} = 0 \\
f_D c_D - f_D c_3 - b c_{1,part} + a_2 c_{1,part} - E_2(c_3 - c_2) = 0 \\
f_{SInp}(c_{SInp,part} + c_{SInp,diss}) - f_{SOut}(c_{1,part} + c_{1,diss}) + f_I c_I + f_D c_D - b c_{1,part} = 0 \\
\alpha c_{1,diss} = f_{SInp} c_{SInp,part} - f_{SOut} c_{1,part} - a_1 c_{1,part}
\end{aligned} \tag{6}$$

Model parameters

Field estimates are available for some of the parameters in equations 6, and their values and source are compiled in Table A1. For surface freshwater inputs at the western edge of the Lower Estuary, we use the sum of estimates at Quebec City and from the Saguenay River. The volume input flow from the Gulf to the Lower Estuary at depth (layers 2 and 3 in Fig. 3) is poorly constrained. The available estimates come from an evaluation of the deep-water advection velocity based on the temperature rise phase-lag (Bugden, 1991; Gilbert, 2004), a circulation model (Galbraith et al., 2016) and a box model (Savenkoff et al., 2001), and range from 4.75×10^4 to 7.5×10^4 $\mathrm{m^3s^{-1}}$. Here, we use a value derived from a mass balance of salinity inputs and outputs ($\sum f_i S_i = 0$), 8.3×10^4 $\mathrm{m^3s^{-1}}$. We obtain the same value using a mass balance of water stable oxygen isotopic compositions. This value fits within the upper range of available estimates (see Table 3). This volume is split between the input to the deep layer and to the CIL is based on the cross-section area of both layers. The remaining parameters (turbulent mixing rates E_1 and E_2, and particle fluxes P_1 and P_2 for each nutrient) are obtained from reverse modeling. Details of these derivations can be found in appendix B. The resulting parameters are given in Table 2, and are well within the range of available field observations (Table 3).

This completes the *present-day* nutrient budget, shown in Fig. 4, for N, P, and Si. To use the model under various perturbation scenarios, a linear relation between the surface nutrient uptake and surface particulate nutrient concentration ($G = \alpha c_{1,diss}$) is obtained, where α is a coefficient of units $\mathrm{m^3s^{-1}}$. The particle settling rate ($P_i = a_i c_{1,part}$) and the sedimentation rate ($S = b c_{1,part}$) are also expressed as a flux of the surface particulate nutrient concentration. Those parameters are presented in Table 2. The flow chart in Fig. 5 depicts how each parameter of the model is obtained.

Validation

The model is validated using historical data. When the nutrient input concentrations to the surface, intermediate (CIL) and deep waters measured prior to 1985 are fed into the model, the outputs reproduce

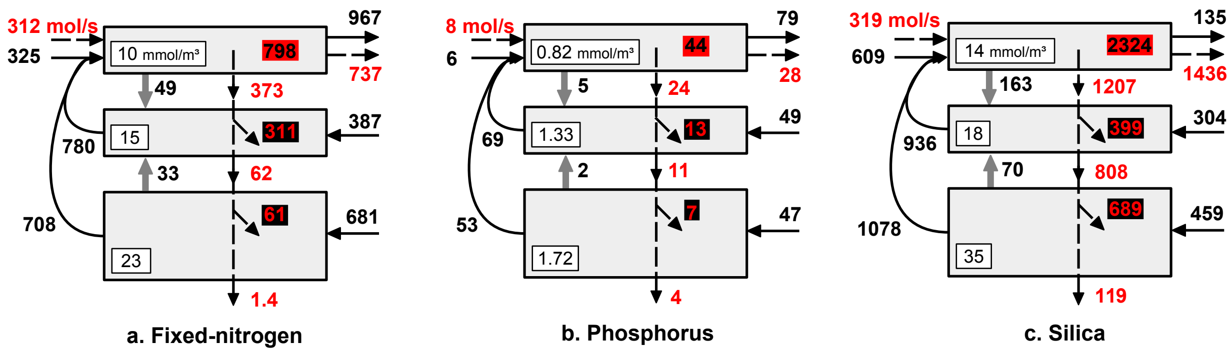

Figure 4: Fluxes of different nutrients in the current steady-state. Values in the white boxes are the nutrient concentrations in each layer, in mmol m^{-3}. The other numbers are the different fluxes, in mol s^{-1}. Black and red numbers represent the dissolved and particulate fluxes, respectively. The black on red background is the conversion from dissolved to particulate, and red on black is particulate to dissolved. Continuous arrows are dissolved fluxes, and dashed arrows are particulate fluxes. The net flux associated with turbulent mixing of dissolved nutrients is represented by the semi-transparent arrows.

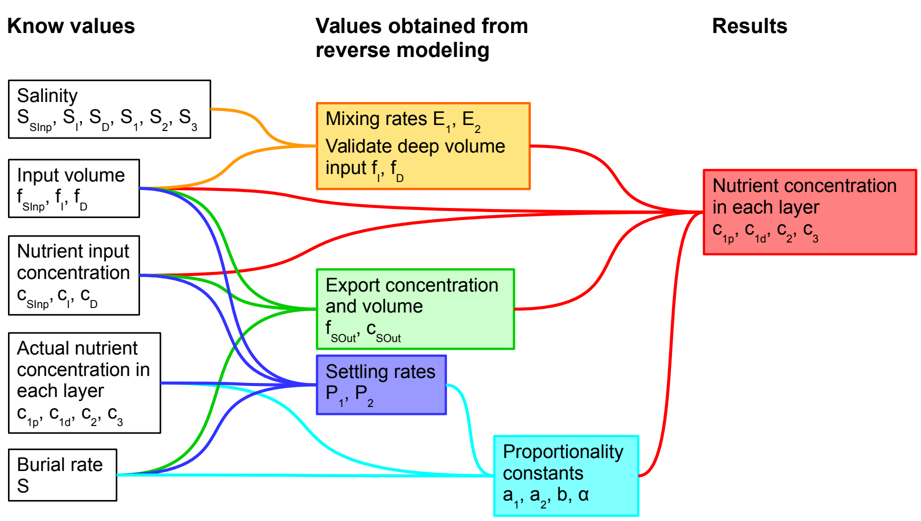

Figure 5: Schematic description of how the value of each parameter of the model is obtained.

the nutrient concentrations in each layer at that time (Table A2). We also tested the theoretical robustness of the model by inducing small perturbations to each of its parameters (Table A3). Perturbations of 1% lead to a maximal variation of 0.9% of the results, implying that the model is robust.

The mixing rates obtained through reverse modeling are sensitive to the different parameters of the model, even if the errors do not propagate to the final model outputs (nutrient concentrations). For example, a 1% perturbation of the salinity value can lead to a 56% error on the mixing rates (see Table A3). This is a theoretical test, since the salinity of each layer is hard to constrain because of spatial variations (see variance in Table A1). The mixing rates obtained from reverse modeling therefore do not have a high enough level of confidence to be considered outside the context of this box model (see Table 3 for a comparison with observations).

4.2. Method for sensitivity analysis

This model is used to study three aspects of nutrient cycling in the LSLE. First, the model is used to test the sensitivity of the system to various theoretical perturbation scenarios. In other words, we used the box model to determine the steady-state nutrient concentrations and fluxes in each layer under varying conditions (dissolved and particulate nutrient inputs at different depths, discharge rate, etc.).

Second, we look at the time evolution of the system towards a new steady-state, following perturbations. To do so, equations are solved in a time-dependent manner, using a finite difference scheme:

$$\frac{dC_i}{dt} = A + B + C + ... \tag{7}$$

as

$$C_i(t+1) = C_i(t) + \Delta t \times [A + B + C + ...] \tag{8}$$

Third, nutrient cycling is related to oxygen consumption in the bottom waters. Eutrophication is defined as the delivery of excess nutrients to surface waters that promotes primary productivity in surface waters, increasing the particulate organic matter (POM) flux towards bottom waters where the organic matter is microbially remineralized, consuming oxygen. Our model computes the flux of POM and remineralization in the LSLE under different environmental conditions. The remineralization rate is related to oxygen consumption by the stoichiometry of the following chemical reaction (Anderson, 1995; Hedges et al., 2002)

$$C_{106}H_{175}O_{42}N_{16}P + 150O_2 + 28H_2O \rightleftharpoons 106HCO_3^- + 16NO_3^- + HPO_4^{2-} + 124H^+ \tag{9}$$

corresponding to a ratio of N:O_2 = 16:150 and P:O_2 = 1:150. Accordingly, in our model, the oxygen consumption rate is given by

$$R_{O_2} = \min[150 \cdot R_P, 150/16 \cdot R_N] \tag{10}$$

where R_{O_2} is the oxygen consumption rate and R_P and R_N are, respectively, the phosphorus and nitrogen remineralization rates obtained from the model. We use the remineralization rates from layer 3 only, as layer

2 is more easily replenished by overlying waters. This rate includes both the pelagic and benthic oxygen respiration rates. Early diagenetic processes (including nutrient release from sediments to the overlying water column) are intrinsically resolved in the model, since the export to sediments is the long-term burial.

Equation 10 yields a present-day oxygen consumption rate of **40 μmol L^{-1} yr^{-1}**. In reality, along the isopycnal where we find the oxygen minimum, oxygen concentrations decrease from 150 μmol L^{-1} at Cabot Strait to 60-70 μmol L^{-1} at the head of the Laurentien Channel following a transit between these two locations of 2 or 4 years (Bugden, 1991; Gilbert, 2004). According to these measurements, a 2 years transit represents an oxygen depletion rate in accordance with the rate obtained from our model. A 4 years transit yields a rate half that from the model (see Table 3). The discrepancy can be attributed to oxygen replenishment from the surface through turbulent mixing. A simple calculation reveals that the discrepancy can be explained by a turbulence coefficient $\mathcal{O}(10^{-5})$ m$^2 s^{-1}$ (1.1×10^{-5} m$^2 s^{-1}$), in agreement with observational (Cyr et al., 2015) and reverse modeling (Savenkoff et al., 2001) studies.

In the following section, we present results of the sensitivity analysis, the time to the establishment of new steady-states, and discuss oxygen consumption, preceded by some general observations about the nutrient budget.

5. Results

5.1. General observations

The strongest fluxes or most prominent processes that determine the nutrient concentrations in each layer are the *mass inputs, particle settling, and nutrient uptake at the surface* (Fig. 4). Simple mass balance informs us that 70% of the fixed-nitrogen and 90% of the phosphorus reaching the surface waters in the LSLE originate from the **deep waters** (both deep and CIL). This implies that nutrients of anthropogenic origin, entering the system through the St. Lawrence River, contribute marginally to the surface-water nutrient pool and can only have a moderate impact on eutrophication rates. Accordingly, respectively 3 and 7 times more particulate and dissolved nutrients reach the Gulf from the LSLE than what is delivered to the Lower Estuary from the St. Lawrence River. This is consistent with studies (Savenkoff et al., 2001; Coote and Yeats, 1979) that describe the LSLE as a 'nutrient pump' which sustains the primary productivity in the Gulf (Steven, 1971). Our estimate of nutrient export towards the Gulf is, however, 70 times larger than the Cyr et al. (2015) estimate based on a balance of turbulent fluxes.

5.2. Sensitivity analysis

Below, we describe the sensitivity of nutrient concentrations in each layer to different perturbations of the fixed-nitrogen inputs, as the other nutrients (phosphorus and silica) show similar responses to the same perturbations.

Changing the dissolved and particulate nitrogen inputs from the St. Lawrence (and Saguenay) River (F_{SInp}) affects the nitrogen concentration in all layers. Fig. 6a shows the steady-state dissolved and particulate fixed-nitrogen concentrations (y-axis) in each layer for a range of riverine particulate plus dissolved nutrient concentrations (x-axis). The present state is designated by the grey band. Quantitatively, a doubling of the inputs of both forms of riverine fixed-nitrogen concentrations leads to a one-third as high increase of both forms of fixed-nitrogen concentrations in the LSLE's surface layer, a one-fifth as high increase in the intermediate layer, and a one-twentieth increase in the deep layer.

A 100% increase (doubling) of the *intermediate* layer nutrient input concentrations increases the dissolved nutrient concentration of surface, intermediate and deep layers respectively by $\sim$ 30%, 60% and 5% (Fig. 6b), while a 100% increase in the *deep* layer input concentration leads to increases of, respectively, $\sim$ 50%, 20% and 85% in the same layers (Fig. 6d). The redistribution of fixed-nitrogen occurs through surface upwelling, affecting the surface nutrient uptake (G in Fig. 6c). The differential response of the system to increased nutrient inputs from the intermediate (CIL) and deep layers is due to the difference in input volume at depth (respectively 54% and 32% of the total volume of water supplied to the LSLE). In summary, variations of both the *riverine* and *deep-water* fixed-nitrogen concentrations have about the same impact on surface water nutrient concentrations.

Finally, modifying the river *volume* flux (freshwater discharge rate, f_{SInp}, keeping the nutrient concentration constant) has a non-linear impact on the new steady-states (Fig. 6e), but similar to increasing the riverine nutrient input (Fig. 6a).

5.3. Time to steady-state

Fig. 6f shows the temporal evolution towards steady state of $c_{1,diss}$, $c_{1,part}$, c_2, and c_3 when we instantaneously double the surface input (river discharge) nutrient concentration. The concentrations increase exponentially towards their new steady state. It takes about **0.5 year** for the system to reach 90% of its new steady state. The time evolution is of a similar form for perturbations to other parameters. The response to changes in the deep-water nutrient concentrations is a little bit slower, requiring **1.2 years** for a doubling of the concentration.

5.4. Oxygen and eutrophication

The deep-water oxygen consumption rate varies linearly with changes in river and deep-water fixed-nitrogen concentrations (Fig. 7). A 100% increase (doubling) in the river (surface) fixed-nitrogen concentration leads to a 50% increase in the deep-water oxygen consumption rate. A 100% increase in the deep-water input fixed-nitrogen concentration, which eventually upwells to the surface, leads to an increase of the deep-water oxygen consumption rate of 32% (Fig. 7), a positive response, as upon an increase in river export concentration. Perturbations to phosphorus inputs do not affect the oxygen consumption rate at depth. This support the hypothesis that nitrogen acts as a limiting nutrient in the LSLE.

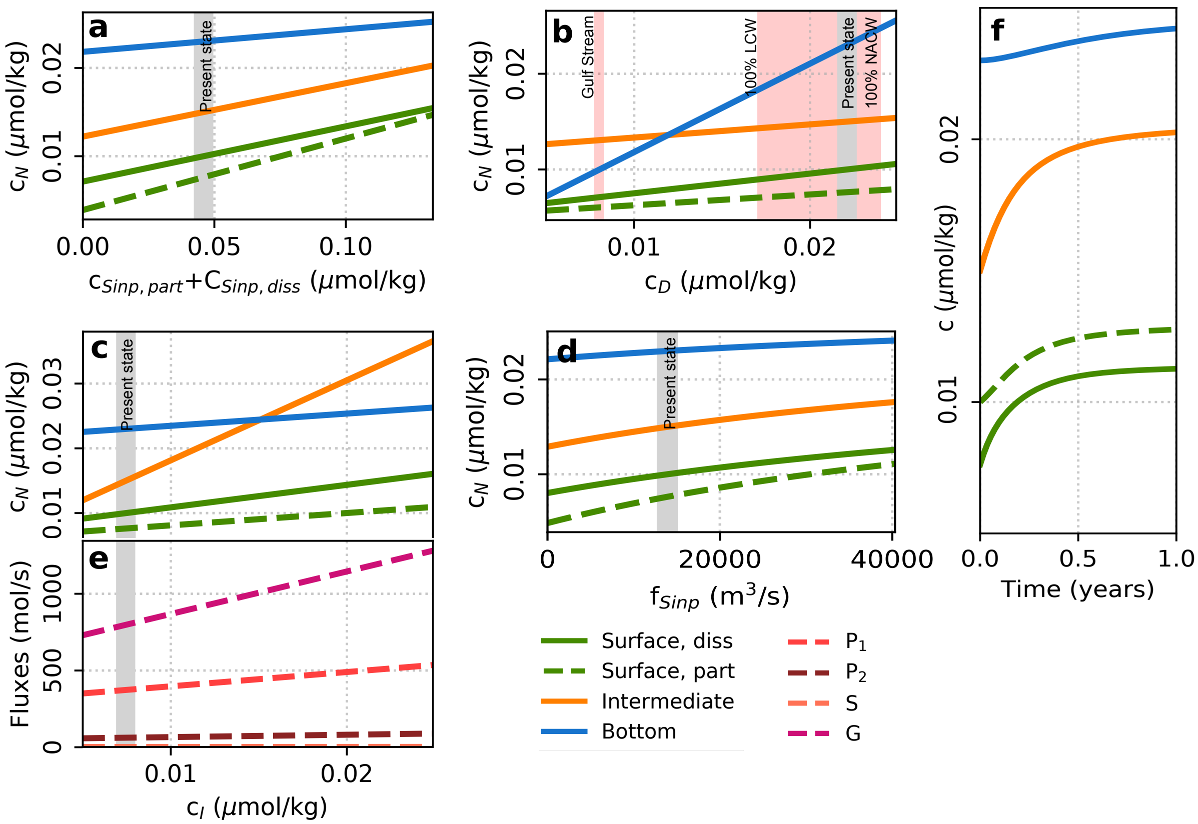

Figure 6: Response of the system to perturbations in **a** dissolved and particulate (in constant proportion) fixed-nitrogen concentrations delivered by waters from the St-Lawrence and Saguenay Rivers (F_{SInp}), **b** intermediate layer input concentrations (F_I), **d** deep layer input concentrations (F_D) and **e** volume flux (freshwater discharge rate) from the St. Lawrence and Saguenay Rivers (f_{SInp}). The x-axis shows the range of perturbations applied, with the present conditions indicated by the grey vertical band. The y-axis shows the new steady-state fixed-nitrogen concentrations in each layer, for the associated perturbation. **c** shows the modeled-system response on the particulate fluxes, the burial rate, and uptake rate associated with **b**. The red zone in **d** denotes the range of possible deep-water nutrient concentrations, the concentrations in the source waters of the deep Estuary: the Labrador Current Waters (lower boundary) and the North Atlantic Central Waters (upper boundary). **f** Temporal evolution towards steady state of the system after a doubling of the surface input (river discharge) nutrient concentration. It takes a half a year to reach 90% of the new steady state.

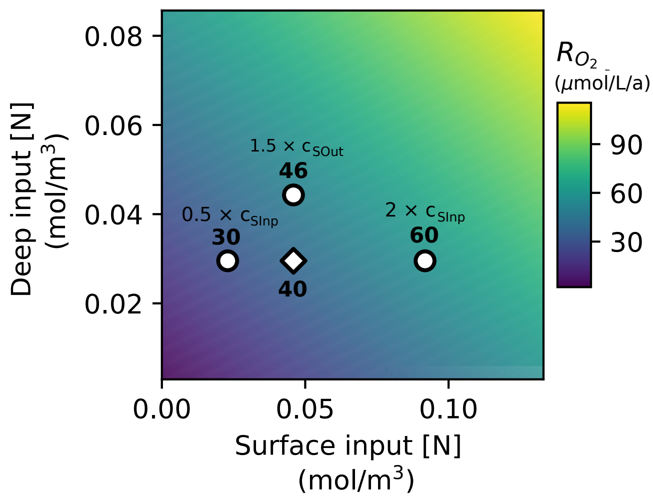

Figure 7: Total oxygen consumption rates in the deep layer (color bar) under a range of perturbations in riverine (x-axis) and deep-water (y-axis) fixed-nitrogen concentrations. The results are the same when changing only nitrogen or nitrogen and phosphorus concentrations. The current state is marked by a 'x'. The stars show some hypothetical scenarios. The negative slope indicates how the expected increase in riverine and in deep-water fixed-nitrogen concentrations add-up to exacerbate entrophication.

6. Discussion

The St. Lawrence River, the most important freshwater tributary to the Lower St. Lawrence Estuary (LSLE), drains dense urban areas and farmed land and is, therefore, highly susceptible to increasing nutrient and organic matter export. Our simple mass balance box model can inform us on how such stresses affect the vertical distribution of nutrients in the LSLE and eutrophication. First, it shows that the LSLE requires little time to reach a new steady-state following perturbations in input fluxes. More importantly, it shows that the impact of anthropogenic nutrient discharge to eutrophication in the LSLE is limited, given that upwelling of deep waters at the head of the Laurentian Channel accounts for nearly 70% of the nitrate input to the surface waters. This result applies to summer conditions. In the winter, the relative contribution of the St. Lawrence River to the surface-water nutrient input is higher, but still not dominant (*Diane Lavoie, personal communication*). Nitrate acts as a limiting nutrient in the LSLE, suggesting that current regulations on phosphate discharge alone are not sufficient to control the level of eutrophication in the LSLE.

Changes in the circulation pattern in the Northwest Atlantic may modify the properties of the bottom waters that enter the Gulf through Cabot Strait and reach the Estuary (Gilbert et al., 2005; Claret et al., 2018). Labrador Current waters (LCW) reaching the continental shelf have lower nutrient concentrations ([NO_3] $\sim$ 17 μM) than deep near-coast Gulf Stream waters that have been enriched by river discharge from the continent ([NO_3] $\sim$ 24 μM, Townsend et al. (2006)), but higher concentrations than pure Gulf Stream waters ([NO_3] $\sim$ 8 μM, (World Ocean Circulation Experiment (WOCE), 2019; Fieux, 2017)). It is unclear whether the expected retreat of the Labrador Current and northern shift of the Gulf Stream (Claret et al., 2018; Caesar et al., 2018) will push more nutrient-rich waters on the continental shelf (Townsend et al., 2006) or will increase the amount of nutrient-poor Gulf Stream water mixing with LCW. Assuming the former, we would expect an increase in the deep-water nutrient input concentrations and, hence, surface nutrient concentrations in the LSLE (Fig. 6bcd), therefore increasing primary production, the particulate organic matter flux to the seafloor, and the microbial respiration rate at depth, adding to allochtonous or anthropogenically-driven eutrophication. Gulf Stream waters also have much lower oxygen concentrations than LCW ($\sim$ 160 μM vs $\sim$ 280 μM, World Ocean Circulation Experiment (WOCE) (2019)), leading to lower oxygen concentrations at Cabot Strait, before the transit to the LSLE during which eutrophication would reduce the oxygen concentrations further.

While it is hard to predict how both river and deep-water fixed-nitrogen concentrations will change in the future, a 50% increase in riverine concentrations and a 25% increase in deep-water concentrations would lead to a 24% increase in the bottom-water oxygen consumption rate, accentuating the stress on the LSLE ecosystems.

Limitation: Deep volume input

As mentioned earlier, the volume of deep-water entering the estuary from the Gulf and Cabot Strait is poorly constrained, even if the simple salinity mass balance calculation used here increases our confidence in the computed volume flux. A different deep-water input would have a strong influence on the model results, as it would change the relative contribution of nutrients of anthropogenic (St. Lawrence River) and North Atlantic origin to the surface waters of the LSLE and their impact on estuarine eutrophication. The amplitude of the impact is visible in Fig. 8. Nevertheless, a better understanding of the circulation in the LC would be desirable to more accurately constrain the nutrient balances in the system.

Other limitations include the linear parameterizations of POM formation and gravitational settling, which would be more realistically represented by non-linear functions. A more complex representation of the circulation and biochemical processes might yield different results.

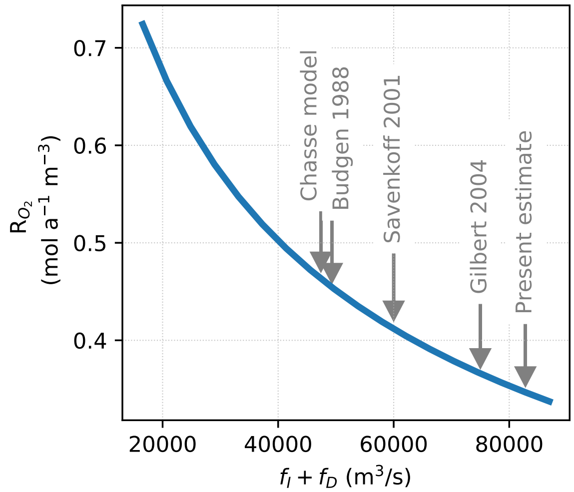

Figure 8: Sensitivity of deep-water oxygen consumption rate to deep-water input volume from the Gulf. Available estimates are shown as dotted lines. The value used here, based on our salinity mass balance calculation, is the last on the right, others are taken from Table 3, whereas the *Chassé model* estimate is taken from Galbraith et al. (2016).

7. Conclusions

A simple box model of the Lower St. Lawrence Estuary (LSLE) is developed to evaluate (i) the sensitivity of the system to perturbations in particulate and dissolved fixed-nitrogen, phosphorus and silica concentrations and water volume inputs, (ii) the time required to reach a new steady-state following a perturbation, and (iii) the sensitivity of the bottom-water oxygen consumption rate. The model is composed of 3 boxes, representing the relatively uniform stratification in that region along the Laurentian Channel during the ice-free season. The model is expressed in terms of a balance of fluxes between each box, namely volume fluxes (input, output and upwelling), net turbulent mixing flux, biogenic particle settling and sediment burial, and ensures mass conservation with nutrient uptake at the surface and remineralization in the deeper layers.

The nutrient budget shows that mass inputs, particle settling, and nutrient uptake at the surface are the most important drivers of nutrient cycling in the LSLE. Three to seven times more nutrients leave the LSLE towards the Gulf than what enters through river input, implying that the LSLE acts as a nutrient pump for the Gulf. Model results indicate that 70% of fixed-nitrogen and 90% of phosphorus in the surface layer originate from deeper waters through upwelling. Hence, the contribution of river discharge to eutrophication is dampened by this large amount of nutrients upwelled to the surface. A doubling of the nutrient river export leads to less than a 0.50-fold increase in bottom-water oxygen consumption rate through eutrophication. Model results reveal that expected changes in circulation in the Northwest Atlantic (decrease Labrador Current waters reaching the mouth of the LC) will contribute to eutrophication in the LSLE, adding to that promoted by rising nutrient input from the St. Lawrence River.

Our box model can be used to address a number of practical problems, such as the impact of changing regulations on water quality, dam volume control, agriculture fertilizer runoff, etc. A similar model can also be developed for other enclosed systems of relatively uniform stratification.

8. Acknowledgements

This project was funded by the DFO-NSERC SECO.net network program. MJ thanks Hydro-Quebec for graduate scholarships.

Table 2: Model parameter values obtained from reversed modeling

Parameter	**Value**
Turbulent mixing rates	($m^3\ s^{-1}$)
E_1, mixing rate at 50 m	-9800
E_2, mixing rate at 150 m	4100
Settling flux coefficient ($P_i = a_i c_{1,part}$)	($m^3\ s^{-1}$)
$a_{1,N}$, for N at 50 m	49000
$a_{2,N}$, for N at 150 m	8000
$a_{1,P}$, for P at 50 m	83000
$a_{2,P}$, for P at 150 m	38000
$a_{1,Si}$, for Si at 50 m	81000
$a_{2,Si}$, for Si at 150 m	54000
Uptake coefficient at the surface ($G = \alpha c_{1,diss}$)	($m^3\ s^{-1}$)
α_N, for N	8.0×10^4
α_P, for P	5.4×10^4
α_{Si}, for Si	166.0×10^4
Sedimentation flux coefficient ($S = bc_{1,part}$)	($m^3\ s^{-1}$)
b_N, for N	184
b_P, for P	1.3×10^4
b_{Si}, for Si	8000

Table 3: Comparison of parameters obtained from reverse modeling and field estimates, as well as values obtained from the model and field estimates.

Parameter	**Model value**	**Field estimates**	**Sources of field estimate**
Export to the Gulf	(mol s^{-1})	(mol s^{-1})	
$F_{SOut,diss}$	967	108	Sinclair et al. (1976), in front of Rimouski
Deep volume input	(m^3 s^{-1})	(m^3 s^{-1})	
$f_I + f_D$, volume input at depth	8.28 $\times 10^4$	4.74×10^4 4.93×10^4 6.0×10^4 7.5×10^4	Chasse model, Galbraith et al. (2016) Bugden (1991) Savenkoff et al. (2001) Gilbert (2004)
Turbulent mixing rates	(m^3/s)	(m^3/s)	
$E_{1,2}$, mixing rate at (50,150) m	$\mathcal{O}(10^3)$, unreliable	1100	Cyr et al. (2015)
Particulate settling rates	(mol s^{-1})	(mol s^{-1})	
$P_{1,N}$, particulate flux of N at 50 m	373	-	
$P_{2,N}$, particulate flux of N at 150 m	62	(**183** $\pm$ 108)	Colombo et al. (1996), integrated over the domain using a linear increase between the two sampled sites
$P_{1,P}$, particulate flux of P at 50 m	24	-	
$P_{2,P}$, particulate flux of P at 150 m	11	(**17** $\pm$ 10)	Colombo et al. (1996) and BioChem database P:N ratio
$P_{1,Si}$, particulate flux of Si at 50 m	1207	-	
$P_{2,Si}$, particulate flux of Si at 150 m	808	(**222** $\pm$ 131)	Colombo et al. (1996) and BioChem database Si:N ratio
O_2 consumption rate at depth	(μmol L^{-1} yr^{-1})	(μmol L^{-1} yr^{-1})	
Rate	40	42 21	4 years transit 2 years transit

Appendix A Supplementary figures and tables

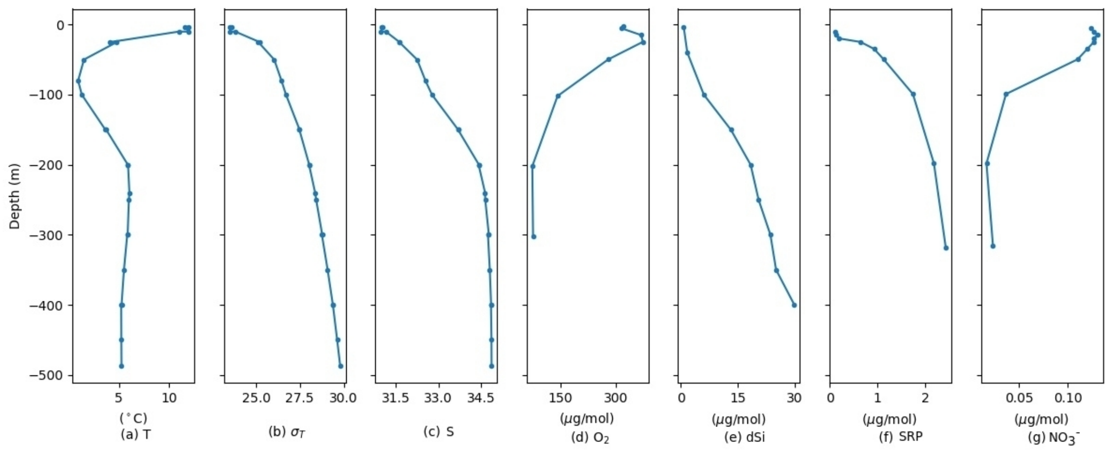

Figure 9: Vertical stratification of the St. Lawrence Lower Estuary. Typical vertical profiles of (a) temperature (T), (b) density (σ_T), (c) practical salinity (S_P), (d) dissolved oxygen (O_2), (e) dissolved silicate (dSi), (f) soluble reactive phosphate (SRP) and (g) nitrate (NO_3^-) in the Lower St. Lawrence Estuary.

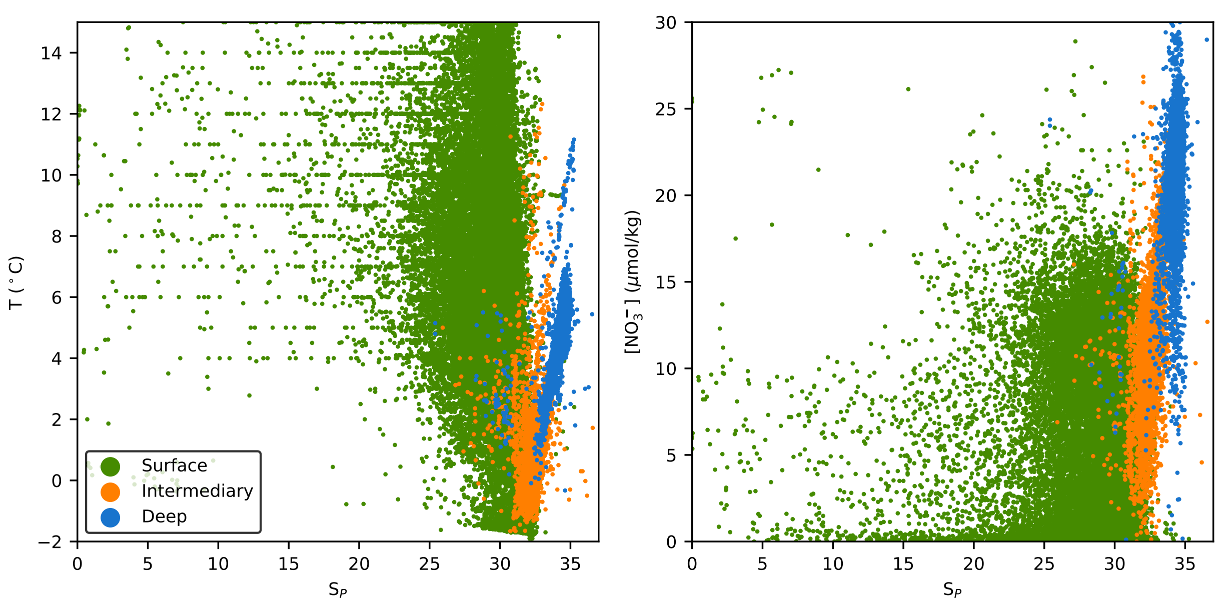

Figure 10: Property-salinity diagrams of combined BioChem and R/V Coriolis II data in the LSLE. The layers are defined as follows: surface: $<$ 40 m, CIL: 60 – 100 m, deep layer: $>$ 150 m. These are the depth ranges that provide the best separation between the layers when we consider the vertical profiles and property-property diagrams.

Table A1: Model parameter values from field observations. We indicate the standard deviation. CI designates the confidence interval.

Parameter	Value	Source
Volume fluxes	($m^3 s^{-1}$)	
f_{SInp}, freshwater input at the western edge	(**1.39** $\pm$ 0.16) $\times 10^4$	Hudon et al. (2017) and Paul del Giorgio (personal communication)
f_D, volume input at the eastern edge, below 150 m	(**3.08** $\pm$ 0.16) $\times 10^4$	Mass balance
f_I, volume input at the eastern edge, between 50 and 150 m	(**5.2** $\pm$ 0.6) $\times 10^4$	Mass balance
Input flux nutrients	(mol m^{-3})	
$c_{SInp,N,diss}$, concentration of dissolved N in surface input water	(**23.4** $\pm$ 0.2) $\times 10^{-3}$ at 95% CI	Hudon et al. (2017)
$c_{SInp,N,part}$, concentration of particulate N in surface input water	(**22.5** $\pm$ 1.8) $\times 10^{-3}$ at 95% CI	"
$c_{SInp,P,diss}$, concentration of dissolved P in surface input water	(**4.52**$\pm$0.04)$\times 10^{-4}$ at 95% CI	"
$c_{SInp,P,part}$, concentration of particulate P in surface input water	(**5.81**$\pm$0.06)$\times 10^{-4}$ at 95% CI	"
$c_{SInp,Si,diss}$, concentration of dissolved Si in surface input water	(**43.8** $\pm$ 1.2) $\times 10^{-3}$	Dinauer and Mucci (2018)
$c_{SInp,Si,part}$, concentration of particulate Si in surface input water	(**11** $\pm$ 5) $\times 10^{-3}$	105:20 ratio with C, from Coote and Yeats (1979) – not precise
$c_{I,N}$, concentration of N in intermediate (CIL) input water	(**7.44** $\pm$ 1.70) $\times 10^{-3}$	Dinauer and Mucci (2018)
$c_{I,P}$, concentration of P in intermediate (CIL) input water	(**0.95** $\pm$ 0.09) $\times 10^{-3}$	“
$c_{I,Si}$, concentration of Si in intermediate (CIL) input water	(**5.85** $\pm$ 1.10) $\times 10^{-3}$	“
$c_{D,N}$, concentration of N in deep input water	(**22.1** $\pm$ 2.3) $\times 10^{-3}$	“
$c_{D,P}$, concentration of P in deep input water	(**1.54** $\pm$ 0.12) $\times 10^{-3}$	“
$c_{D,Si}$, concentration of Si in deep input water	(**14.9** $\pm$ 4.3) $\times 10^{-3}$	“
Burial rates		
B_N, burial rate of N	**0.35** (0.23–0.7) mg $cm^{-2} yr^{-1}$ = **1.4** (0.9–2.8) mol s^{-1}	Muzuka and Hillaire-Marcel (1999), weighted for LSLE average.
B_P, burial rate of P	**0.49** (0.32–0.66) mg $m^{-2} yr^{-1}$ = **3.8** (2.5–5.1) mol s^{-1}	Louchouarn et al. (1997), Anticosti value adjusted for LSLE.
B_{Si}, burial rate of Si	(**0.5** $\pm$ 0.1) mg $m^{-2} yr^{-1}$ = (**119** $\pm$ 19) mol s^{-1}	Mucci et al. (2003)

Parameter	**Value**	**Source**
Observed conservative tracers values		
S_1, practical salinity in layer 1	(**28** ± 2)	BioChem database
S_2, practical salinity in layer 2	(**32.7** ± 0.4)	"
S_3, practical salinity in layer 3	(**34.2** ± 0.5)	"
S_{SInp}, practical salinity of surface input water	**0**	"
S_D, practical salinity of deep input water	(**34.4** ± 0.6)	"
δ^{18} O$_1$, stable oxygen isotopic comp. of layer 1 (‰)	(**-5.0** ± 1.5)	BioChem database
δ^{18} O$_2$, stable oxygen isotopic comp. of layer 2 (‰)	(**-1** ± 1)	"
δ^{18} O$_3$, stable oxygen isotopic comp. of layer 3 (‰)	(**-0.2** ± 1.0)	"
δ^{18} O$_{SInp}$, stable oxygen isotopic comp. of surface input water (‰)	(**-0.09** ± 0.05)	Dinauer et al. (2017)
δ^{18} O$_D$, stable oxygen isotopic comp. of deep input water (‰)	(**-9.83** ± 0.08)	"
Observed nutrient concentration values	(mol m^{-3})	
$c_{1,N}$, concentration of N in layer 1	(**10** ± 5) $\times 10^{-3}$	BioChem database
$c_{1,P}$, concentration of P in layer 1	(**0.82** ± 7) $\times 10^{-3}$	"
$c_{1,Si}$, concentration of Si in layer 1	(**14** ± 7) $\times 10^{-3}$	"
$c_{2,N}$, concentration of N in layer 2	(**15** ± 3) $\times 10^{-3}$	"
$c_{2,P}$, concentration of P in layer 2	(**1.33** ± 0.2) $\times 10^{-3}$	"
$c_{2,Si}$, concentration of Si in layer 2	(**18** ± 5) $\times 10^{-3}$	"
$c_{3,N}$, concentration of N in layer 3	(**23** ± 2) $\times 10^{-3}$	"
$c_{3,P}$, concentration of P in layer 3	(**1.72** ± 0.57) $\times 10^{-3}$	"
$c_{3,Si}$, concentration of Si in layer 3	(**35** ± 9) $\times 10^{-3}$	"

Appendix B Details of reverse modeling

Below are the steps taken to find the missing parameters by reserve modeling

1. First, the particulate export is found from Eq. 4.1. Using the volume export, this gives the concentration of particulate nutrients in the first layer.
2. Second, the mixing rates are found from reverse modeling. To do so, we solve Eq. 1 for E_1 and Eq. 3 for E_2 for salinity, using field measurements of salinity given in Table A1 and removing all terms related to particulate matter. This gives :

$$E_1 = \frac{-f_{SInp}S_{SInp} + f_{SOut}S_1 - f_I S_2 - f_D S_3}{S_2 - S_1}$$
$$E_2 = \frac{f_D S_D + f_D S_3}{S_3 - S_2}$$

3. Settling rates are derived from reverse modeling for each element. To do so, we solve the system of equations formed of equations 1 and 3 for P_1 and P_2. This will be of the form:

$$\begin{pmatrix} 1 & 0 \\ 0 & -1 \end{pmatrix} \begin{pmatrix} P_1 \\ P_2 \end{pmatrix} = \begin{pmatrix} f_{SInp}(c_{SInp,diss} + c_{SInp,part}) - f_{SOut}(c_{1,diss} + c_{1,part}) + f_I c_2 + f_D c_3 + E_1(c_2 - c_{1,diss}) \\ f_D c_D - f_D c_3 - E_2(c_3 - c_2) - B \end{pmatrix}$$

Appendix C Details of model solving

Below we describe how we solve the model (retrieve the steady-state concentration values in each layer) under different sets of conditions.

With the four unknowns being the three layers' nutrient concentrations with particulate and dissolved form in the first layer, we solve the system formed of Equations 6 according to:

$$\begin{pmatrix} E_1 + f_{SOut} & a_1 + f_{SOut} & -E_1 - f_I - f_D & 0 \\ 0 & b - a_2 & -E_2 & f_D + E_2 \\ f_{SOut} & f_{SOut} + b & 0 & 0 \\ \alpha & f_{SOut} + a_1 & 0 & 0 \end{pmatrix} \begin{pmatrix} c_{1,diss} \\ c_{1,part} \\ c_2 \\ c_3 \end{pmatrix} = \begin{pmatrix} f_{SInp}(c_{SInp,part} + c_{SInp,diss}) \\ f_D c_D \\ f_{SInp}(c_{SInp,part} + c_{SInp,diss}) + f_I c_I + f_D c_D \\ f_{SInp} c_{SInp,part} \end{pmatrix}$$

Appendix D Model validation

Table A2: Historical validation of the box model. Units (μmol m^{-3}). Inputs are the values fed to the model, based on observations from the two time periods. We compare the results from the model with observations of the fixed-nitrogen concentrations in each layer. We see that the two agree.

	Input				**Output**		
	$c_{N,SInp,diss}$	$c_{N,SInp,part}$	$c_{N,I}$	$c_{N,D}$	c_1	c_2	c_3
After 2000	25.5	22.6	7.4	22.1	10	15	23
Prior to 1985	7	6	10	18			
				Calculated	8	14	19
				Observations	8 $\pm$ 4	11 $\pm$ 4	18 $\pm$ 4

Table A3: Robustness of the model: effect of a 1% perturbation of the different parameters on the model outputs. The symbol '$<$' is used when the induced change is less than 0.1%.

Perturbed parameter	Variable affected (%)							
	E_1	E_2	a_1	a_2	$c_{1,diss}$	$c_{1,part}$	c_2	c_3
f_{SInp}	8	-	1.1	$<$	0.3	0.2	$<$	$<$
f_I	5	-	0.4	$<$	0.5	0.1	0.4	0.1
f_D	4	1	0.4	0.4	0.1	0.2	0.1	$<$
S_1	56	0	-	-	-	-	-	-
S_2	28	28	-	-	-	-	-	-
S_3	23	158	-	-	-	-	-	-
S_D	-	172	-	-	-	-	-	-
E	-	-	0.1	0.5	$<$	$<$	0.1	0.1
B	-	-	$<$	$<$	$<$	$<$	$<$	$<$
$c_{SInp,part}$	-	-	0.8	$<$	0.4	$<$	0.1	$<$
$c_{SInp,diss}$	-	-	0.9	$<$	0.1	0.2	$<$	$<$
c_I	-	-	-	-	0.2	0.3	0.8	0.1
c_D	-	-	$<$	11.0	0.3	0.5	0.1	0.9
$c_{1,part}$	-	-	2.0	$<$	-	-	-	-
$c_{1,diss}$	-	-	2.3	$<$	-	-	-	-
c_2	-	-	1.7	1.0	-	-	-	-
c_3	-	-	1.9	13.0	-	-	-	-

References

Anderson, L. A., 1995. On the hydrogen and oxygen content of marine phytoplankton. Deep Sea Research part I: Oceanographic Research Papers 42 (9), 1675–1680.

Benoit, P., Gratton, Y., Mucci, A., 2006. Modeling of dissolved oxygen levels in the bottom waters of the Lower St. Lawrence Estuary: Coupling of benthic and pelagic processes. Marine Chemistry 102 (1-2), 13–32.

Bugden, G. L., 1991. Changes in the temperature-salinity characteristics of the deeper waters of the Gulf of St. Lawrence over the past several decades. In J.-C. Therriault [ed.] The Gulf of St. Lawrence: small ocean or big estuary? Can. Spec. Publ. Fish. Aquat. Sci. 114, 139–147.

Caesar, L., Rahmstorf, S., Robinson, A., Feulner, G., Saba, V., 2018. Observed fingerprint of a weakening Atlantic Ocean overturning circulation. Nature 556, 191–196.

Clair, T. A., Dennis, I. F., Bélanger, S., 2013. Riverine nitrogen and carbon exports from the canadian landmass to estuaries. Biogeochemistry 115 (1-3), 195–211.

Claret, M., D., G. E., Palter, J. B., D., B., Fennel, K., Gilbert, D., Dunne, J. P., 2018. Rapid coastal deoxygenation due to large scale ocean circulation shift in the northwest Atlantic. Nature Climate Change 8, 868–872.

Colombo, J., Silverberg, N., Gearing, J., 1996. Biogeochemistry of organic matter in the laurentian trough, ii. bulk composition of the sediments and relative reactivity of major components during early diagenesis. Marine Chemistry 51 (4), 295–314.

Coote, A., Yeats, P., 1979. Distribution of nutrients in the Gulf of St. Lawrence. Journal of the Fisheries Board of Canada 36 (2), 122–131.

Cyr, F., Bourgault, D., Galbraith, P. S., Gosselin, M., 2015. Turbulent nitrate fluxes in the Lower St. Lawrence Estuary, Canada. Journal of Geophysical Research: Oceans 120 (3), 2308–2330.

Dickie, L. M., Trites, R. W., 1983. The Gulf of St. Lawrence. In: Ketchum, B. H. (Ed.), Ecosystems of the World: Estuaries and Enclosed Seas. Elsevier, Amsterdam.

Dinauer, A., Mucci, A., 2018. Distinguishing between physical and biological controls on the spatial variability of pCO2: A novel approach using omp water mass analysis (St. Lawrence, Canada). Marine Chemistry 204, 107–120.

Dunne, J. P., Armstrong, R. A., Gnanadesikan, A., Sarmiento, J. L., 2005. Empirical and mechanistic models for the particle export ratio. Global Biogeochemical Cycles 19 (4).

Fieux, M., 2017. The Planetary Ocean. EDP Sciences.

Galbraith, P. S., 2006. Winter water masses in the Gulf of St. Lawrence. Journal of Geophysical Research: Oceans 111 (C6).

Galbraith, P. S., Chassé, J., Gilbert, D., Larouche, P., Brickman, D., Pettigrew, B., Devine, L., Gosselin, A., Pettipas, R., Lafleur, C., 2016. Physical oceanographic conditions in the Gulf of St. Lawrence in 2016. Canadian Science Advisory Secretariat.

Genovesi, L., De Vernal, A., Thibodeau, B., Hillaire-Marcel, C., Mucci, A., Gilbert, D., 2011. Recent changes in bottom water oxygenation and temperature in the Gulf of St. Lawrence: Micropaleontological and geochemical evidence. Limnology and Oceanography 56 (4), 1319–1329.

Gilbert, D., 2004. Propagation of temperature signals along the northwest Atlantic continental shelf edge and into the Laurentian Channel. In: Abstract, ICES CIEM Annual Science Conference September. pp. 22–25.

Gilbert, D., Sundby, B., Gobeil, C., Mucci, A., Tremblay, G.-H., 2005. A seventy-two-year record of diminishing deep-water oxygen in the St. Lawrence estuary: The northwest Atlantic connection. Limnology and Oceanography 50 (5), 1654–1666.

Gratton, Y., Mertz, G., Gagné, J. A., 1988. Satellite observations of tidal upwelling and mixing in the st. lawrence estuary. Journal of Geophysical Research: Oceans 93 (C6), 6947–6954.

Hedges, J., Baldock, J., Gélinas, Y., Lee, C., Peterson, M., Wakeham, S., 2002. The biochemical and elemental compositions of marine plankton: A nmr perspective. Marine Chemistry 78 (1), 47–63.

Hudon, C., Gagnon, P., Rondeau, M., Hébert, S., Gilbert, D., Hill, B., Patoine, M., Starr, M., 2017. Hydrological and biological processes modulate carbon, nitrogen and phosphorus flux from the St. Lawrence River to its estuary (Quebec, Canada). Biogeochemistry 135 (3), 251–276.

Kriest, I., Oschlies, A., 2008. On the treatment of particulate organic matter sinking in large-scale models of marine biogeochemical cycles. Biogeosciences 5, 55–72.

Louchouarn, P., Lucotte, M., Duchemin, E., de Vernal, A., 1997. Early diagenetic processes in recent sediments of the Gulf of St-Lawrence: phosphorus, carbon and iron burial rates. Marine Geology 139 (1-4), 181–200.

Marcogliese, D. J., Blaise, C., Cyr, D., De Lafontaine, Y., Fournier, M., Gagné, F., Gagnon, C., Hudon, C., 2015. Effects of a major municipal effluent on the st. lawrence river: A case study. Ambio 44 (4), 257–274.

Martin, J. H., Knauer, G. A., Karl, D. M., Broenkow, W. W., 1987. Vertex: carbon cycling in the northeast pacific. Deep Sea Research Part A. Oceanographic Research Papers 34 (2), 267–285.

Mucci, A., Boudreau, B., Guignard, C., 2003. Diagenetic mobility of trace elements in sediments covered by a flash flood deposit: Mn, Fe and As. Applied Geochemistry 18 (7), 1011–1026.

Muzuka, A. N., Hillaire-Marcel, C., 1999. Burial rates of organic matter along the eastern canadian margin and stable isotope constraints on its origin and diagenetic evolution. Marine Geology 160 (3-4), 251–270.

Painchaud, J., Lefaivre, D., Therriault, J.-C., 1987. Box model analysis of bacterial fluxes in the st. lawrence estuary. Marine Ecology Progress Series. Oldendorf 41 (3), 241–252.

Pocklington, R., Tan, F. C., 1987. Seasonal and annual variations in the organic matter contributed by the St Lawrence River to the Gulf of St. Lawrence. Geochimica et Cosmochimica Acta 51 (9), 2579–2586.

Prospero, J., Barrett, K., Church, T., Dentener, F., Duce, R., Galloway, J., Levy, H., Moody, J., Quinn, P., 1996. Atmospheric deposition of nutrients to the North Atlantic Basin. Biogeochemistry 35 (1), 27–73.

Sarmiento, J. L., Gruber, N., 2006. Ocean Biogeochemical Dynamics. Princeton University Press.

Savenkoff, C., Vézina, A., P.C., S., G., H., 2001. Summer transports of nutrients in the Gulf of St. Lawrence estimated by inverse modelling. Estuarine, Coastal and Shelf Science 52, 565–587.

Sinclair, M., El-Sabh, M. I., Brindle, J.-R., 1976. Seaward Nutrient Transport in the Lower St . Lawrence Estuary Seasonal variability in net volume transport. Canadian Journal of Fisheries and Aquatic Sciences 33, 1271–1277.

Steven, D., 1971. International biological program study of the gulf of st. lawrence. In: Proceedings of the 2nd Gulf of St. Lawrence Workshop. Bedford Inst. of Oceanogr Dartmouth, NH, Canada, pp. 146–159.

Thibodeau, B., de Vernal, A., Mucci, A., 2006. Recent eutrophication and consequent hypoxia in the bottom waters of the Lower St. Lawrence Estuary: Micropaleontological and geochemical evidence. Marine Geology 231 (1-4), 37–50.

Thibodeau, B., Lehmann, M. F., Kowarzyk, J., Mucci, A., Gélinas, Y., Gilbert, D., Maranger, R., Alkhatib, M., 2010. Benthic nutrient fluxes along the Laurentian Channel: impacts on the N budget of the St. Lawrence marine system. Estuarine, Coastal and Shelf Science 90 (4), 195–205.

Townsend, D. W., Thomas, A. C., Mayer, L. M., Thomas, M. A., Quinlan, J. A., 2006. Oceanography of the northwest atlantic continental shelf (1, w). In: Robinson, A. R., Brink, K. H. (Eds.), The sea: the global coastal ocean: interdisciplinary regional studies and syntheses. Harvard University Press, Ch. 5, pp. 119–168.

World Ocean Circulation Experiment (WOCE), 2019. Woce climatology. http://icdc.cen.uni-hamburg.de/las/getUI.do?dsid=id-3c81c78c2b&catid=9B3B992E6DA90BD12ED57F84FE8364BC&varid=TEMP-id-3c81c78c2b&plot=XY_zoomable_image&view=xy&auto=true, accessed: 2019-03-05.